CALPHAD: Computer Coupling of Phase Diagrams and Thermochemistry 42 (2013) 27–37

Contents lists available at ScienceDirect

CALPHAD: Computer Coupling of Phase Diagrams and Thermochemistry

journal homepage: www.elsevier.com/locate/calphad

Experimental investigation and first-principle calculations coupled with thermodynamic modeling of the Mn–Nd phase diagram

A.O. Mostafa [a], A.E. Gheribi [b], D. Kevorkov [a], Md. Mezbahul-Islam [a], M. Medraj [a,*]

[a] Department of Mechanical and Industrial Engineering, Concordia University, 1455 Maisonneuve Blvd. W., Montreal, QC, Canada H3G 1M8
[b] CRCT—Centre for Research in Computational Thermochemistry, Department of Chemical Engineering, École Polytechnique de Montréal, C.P. 6079, Succursale Centre-Ville, Montréal, QC, Canada H3C 3A7

ARTICLE INFO

Article history:
Received 5 March 2013
Received in revised form
28 May 2013
Accepted 9 July 2013
Available online 1 August 2013

Keywords:
Diffusion couples
Experimental investigation
First-principles calculations
Thermodynamic modeling
Mn–Nd phase diagram

ABSTRACT

The complete Mn–Nd phase diagram was established experimentally by means of key samples and diffusion couple techniques. The phase transformation temperatures, crystal structures and phase equilibria were studied using differential scanning calorimetry (DSC), X-ray diffraction (XRD), electron probe microanalysis (EPMA), and scanning electron microscope (SEM) techniques. Three compounds in the Mn-rich side and two terminal solid solutions in the Nd-rich side were observed. The compounds Mn_2Nd, $Mn_{23}Nd_6$, and $Mn_{17}Nd_2$ form peritectically at 850, 940, and 1025 °C, respectively. The eutectoidal decompositions of the compounds, Mn_2Nd, and $Mn_{23}Nd_6$, were confirmed in the temperature ranges of 650–550 and 550–400 °C, respectively, using EPMA. The maximum solubility of Mn in DHCP-Nd was found to be 2.3 at% Mn at the 685 °C eutectic temperature. The solvus line of DHCP-Nd was determined using EPMA. The solubility of Mn in BCC-Nd was extrapolated from DSC data to be 5.0 at% Mn at 728 °C. The existence of a $Mn_{17}Nd_2$ phase of the Th_2Ni_{17} type structure was confirmed using EPMA and XRD. The system was modelled using CALPHAD methodology. The quasi-chemical model (QCM) was used to describe the liquid phase, the terminal solution phases were modeled as substitutional solutions using the random mixing model, and the intermetallic compounds were treated as stoichiometric phases. The enthalpies of formation of the system compounds were calculated using the electronic density functional method. The resulting enthalpy of mixing was in good agreement with the literature.

1. Introduction

Manganese is used mainly as a deoxidizer and desulfurizer element in the steel, cast iron, and non-ferrous industries. For this reason it is also called a cleaning agent [1]. Mn alloyed with steel provides very tough, wear resistant, and ferromagnetic alloys [2]. Furthermore, addition of Mn to Mg alloys improves their hot and cold strengths, resistance to corrosion, and formability. Due to its high reactivity with other elements, manganese phase diagrams usually show very complicated sequences of intermediate phases. Thus, when manganese is alloyed with various rare earth elements (RE), a significant variation in the properties is obtained [3]. The crystal structures of the phases formed in some Mn–RE systems are listed in Table 1 [4–9]. Addition of Nd to Mg–Mn alloys develops their microstructures, with regard to grain size, and the resulting mechanical properties during indirect extrusion processes. Nd is considered the stronger texture modifier of Mg–Mn alloys compared to other REs, such as Ce [10].

Binary systems of Mn with heavy RE metals exhibit increasing number of stable intermetallic compounds. The Mn–Nd phase diagram was first investigated experimentally by Kirchmayr and Lugscheider [11] using DTA and XRD. According to these authors, the eutectic occurs at 700 °C and 27 at% Mn; a negligible terminal solid solubility near the Nd side was considered. Three peritectically melting compounds, Mn_2Nd ($L+Mn_{23}Nd_6 \Leftrightarrow Mn_2Nd$, at 920 °C), $Mn_{23}Nd_6$ ($L+Mn_{12}Nd \Leftrightarrow Mn_{23}Nd_6$, at 975 °C) and $Mn_{12}Nd$ ($L+\beta\text{-}Mn \Leftrightarrow Mn_{12}Nd$, at 1100 °C) were observed. Two compounds ($Mn_{23}Nd_6$ and $Mn_{12}Nd$) were confirmed with certainty. No evidence of Mn_2Nd existence was obtained by Kirchmayr and Lugscheider [11] using diffraction methods; it was suggested from DTA only and shown by dashed lines in Fig. 1(a). The compound Mn_2RE, having a 2:1 stoichiometric ratio, was observed and reported to occur in two structure types: hexagonal $MgZn_2$ ($a=5.574$ Å and $c=9.082$ Å) at room temperature and monoclinic $MgCu_2$ ($a=5.544$ Å, $b=9.721$ Å, $c=9.013$ Å, and $\gamma=89.8°$) at −169 °C [5,7,12]. Another version of Mn–Nd phase diagram was introduced by Makhalenko and Kuz′ma [13] by means of X-ray diffraction, Fig. 1(b). Two intermediate phases, Mn_2Nd and $Mn_{23}Nd_6$, were observed. In contrast with Kirchmayr and Lugscheider [11], Mn_2Nd was described as a laves phase with narrow range of temperature for its stability and

* Corresponding author. Tel.: +1 514 848 2424x3146; fax: +1 514 848 3175.
E-mail address: mmedraj@encs.concordia.ca (M. Medraj).

0364-5916/$ - see front matter © 2013 Elsevier Ltd. All rights reserved.
http://dx.doi.org/10.1016/j.calphad.2013.07.004

Table 1
Possible structural phases formed in Mn–RE systems [4–9].

Stoichiometry	Condition	Rare earth element (M)	Prototype
Mn_3M_4	High pressure	Yb	Co_3Ho_4
Mn_2M	High temperature	Sc, Nd, Sm, Er, Tm, Lu	$MgZn_2$
		Y, Gd, Tb, Dy, Ho	Cu_2Mg
	Low temperature	Sc, Ho, Er, Tm, Lu	$MgZn_2$
		Gd, Tb, Dy, Nd	Cu_2Mg
		Sm	
	High pressure	Yb, Y, Gd, Tb, Dy, Ho	$MgZn_2$
$Mn_{23}M_6$	High temperature	Y, Pr, Nd, Sm, Gd, Tb, Dy, Ho, Er, Tm, Lu	$Mn_{23}Th_6$
	Low temperature	Y, Sm, Gd, Tb, Dy, Ho, Er, Tm, Lu	
	High pressure	Yb	
Mn_5M		Lu	$LuMn_5$
$Mn_{17}M_2$	High pressure	Yb	$Ni_{17}Th_2$
$Mn_{12}M$		Y, Gd, Tb, Dy, Ho, Er, Tm	$Mn_{12}Th$

undergoes eutectoid decomposition at ~650 °C. Moreover, $Mn_{23}Nd_6$ was found in the range from 975 to 600 °C and to undergo eutectoid decomposition [13]. The liquidus line was modified by Okamoto [14,15], considering the requirements for the initial slopes of the terminal solid solutions, assuming similarity with the Mn–Pr system. Saccone et al. [4] reinvestigated the 10 to 85 at% Mn partial Mn–Nd phase diagram using SEM, DTA and XRD, as shown in Fig. 1 (c). They reported that Mn_2Nd and $Mn_{23}Nd_6$ formed peritectically at 820 and 930 °C, respectively. Mn_2Nd and $Mn_{23}Nd_6$ were tentatively suggested to decompose eutectoidally at ~580 and ~480 °C, respectively. However, Liu et al. [16] using X-ray diffraction reported the existence of $Mn_{12}Nd$ intermetallic at 500 °C. Based on the DTA results of Saccone et al. [4], the liquidus line was significantly lowered compared to that in both [11] and [13] phase diagrams.

Recently, the enthalpy of mixing of the liquid phases in the Mn–Nd system was determined by Ivanov et al. [17] using isoperibolic calorimetry. The obtained curve showed minimum and maximum at 90 and 40 at% Mn, respectively. More recently, the system was modeled by Kim and Jung [18]. In their model, they adopted the experimental results obtained by Saccone et al. [4], because these results were more reliable from the thermodynamics point of view. They [18] assumed a solid solubility of 4.0 at % Mn in BCC-Nd at 736 °C.

The experimental data available in the literature were contradictory, and therefore, different Mn–Nd phase diagram versions were put forward. Moreover, no concrete knowledge of the phase equilibria at the composition extremes was established. The purpose of this work is to construct a self-consistent Mn–Nd phase diagram experimentally by means of key samples and diffusion couple techniques, using ICP, XRD, DSC, and SEM/EPMA. First-principles calculations were employed to determine the enthalpies of formation of the system compounds. All the information obtained from this work as well as from the literature has enabled a complete thermodynamic optimization of this system.

2. Experimental work

The starting materials were Mn metal flakes (purity, 99.95 wt%) and Nd metal ingots (purity, 99.9 wt%) supplied by Alfa Aesar®, Johnson Matthey Company, Inc. Alloys (3–4 gm) were prepared using an arc-melting furnace under argon atmosphere. The samples were melted in a water-cooled copper crucible using a non-consumable tungsten electrode. Every alloy was melted several times to ensure homogeneity. The actual global composition was chemically determined using an ULTIMA2 optical emission spectrometer (OES) ICP. The samples were dissolved in concentrated

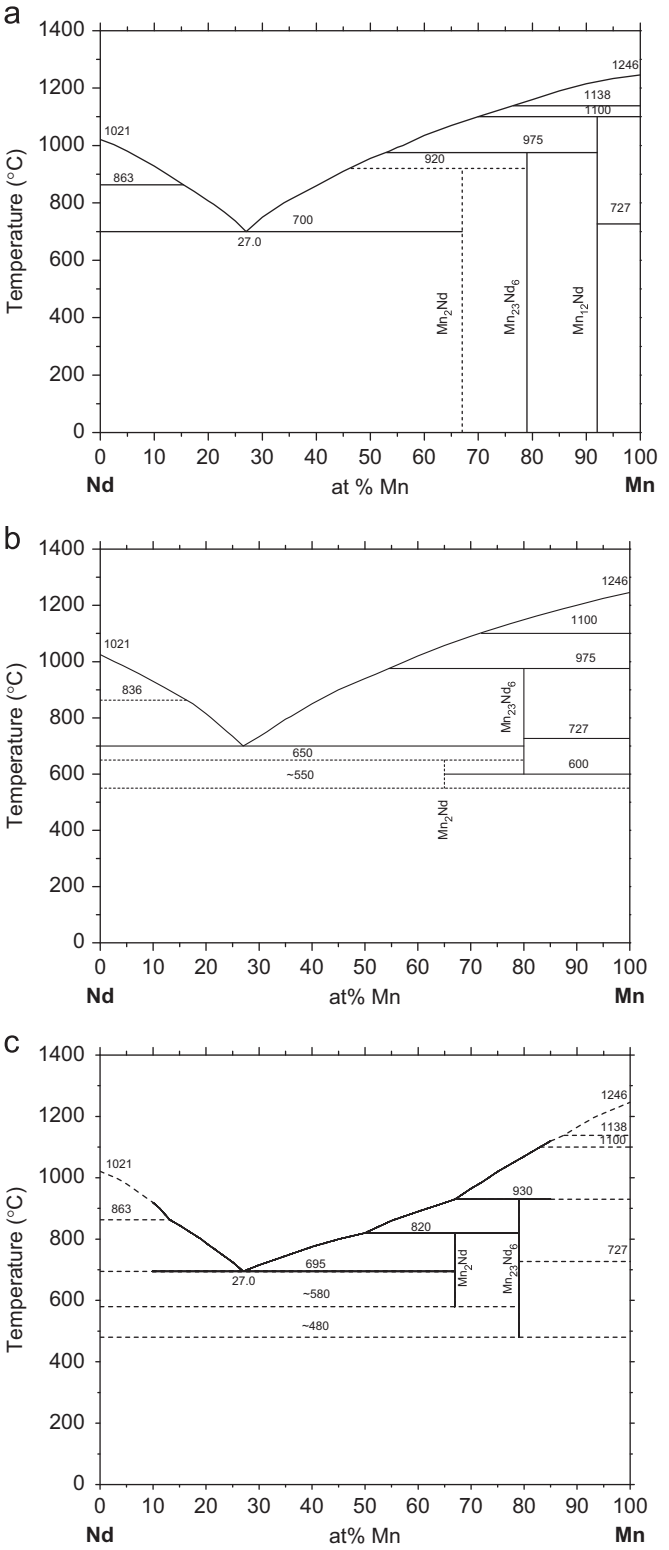

Fig. 1. The Mn–Nd phase diagrams established by (a) Kirchmayr and Lugscheider [11], (b) Makhalenko and Kuz′ma [13], and (c) Saccone et al. [4].

HNO_3. The as-cast samples were cut into several divisions some of which were placed in sealed alumina crucibles for thermal analysis using SETARAM-Setsys1200 differential scanning calorimeter (DSC) for investigating the phase transformation and melting temperatures. Different heating and cooling rates of 1, 5, 10 and 15 °C/min were attempted for the DSC experiments to

obtain the optimum rate for the current system. Low speeds increase the contact time between the liquid alloy and the alumina crucible which increases the chance of reaction between them. Therefore, a scanning speed of 10 °C/min was used for all the alloys except the eutectic composition where 15 °C/min was used to minimize the effect of reaction between the liquid and the crucible. The DSC cycles were repeated at least three times for each sample to ensure the reproducibility of the results. In the present work, the results of thermal analysis obtained using graphite crucibles were omitted. Additional DSC peaks representing high melting temperature carbides were detected. Hence, alumina crucibles were used instead. Fig. 2(a) shows the DSC results of the eutectic sample composed of 27.8 at% Mn using 15 °C/min heating and cooling rates in an alumina crucible. One endothermic peak and one exothermic peak were observed during heating and cooling cycles. The eutectic temperature was recorded from the onset of the heating and cooling peaks. Fig. 2(b) shows the DSC results of the same sample using a graphite crucible. The eutectic temperature was decreased to 674 °C and another peak at relatively high temperature of 873 °C was detected.

Other sample divisions were wrapped in tantalum foil and encapsulated in quartz tubes under argon to be annealed at certain temperature followed by water quenching. The samples were kept on the target temperature for different periods to reach the equilibrium condition. The annealing conditions are listed in Table 2. The quartz tubes remained clear even for the long annealing times; this indicates that evaporation was minimum. Powder XRD analysis was performed from 20 to 120° in 0.02° steps. The alloy powders were prepared in a glove box under argon to prevent sample oxidation. The XRD spectra were used to identify the crystal structure of the Mn–Nd system compounds using X'Pert Highscore plus software [19].

Solid–solid diffusion couples were designed to investigate the Mn–Nd phase equilibria at 650 °C. The contact surfaces of the pure Mn and Nd end-members were grinded down gradually starting from 120 up to 1200 grit SiC paper. 99% pure ethanol was used as lubricant, due to the high susceptibility of Nd and Mn to oxidation. The grinded samples were then polished gradually from 6μm to 1 μm using an alcohol-based diamond suspension. The polished Mn sample was carefully squeezed between two polished Nd plates in sandwich form using a hydraulic press. Diffusion layers between the equilibrated phases were identified using EPMA.

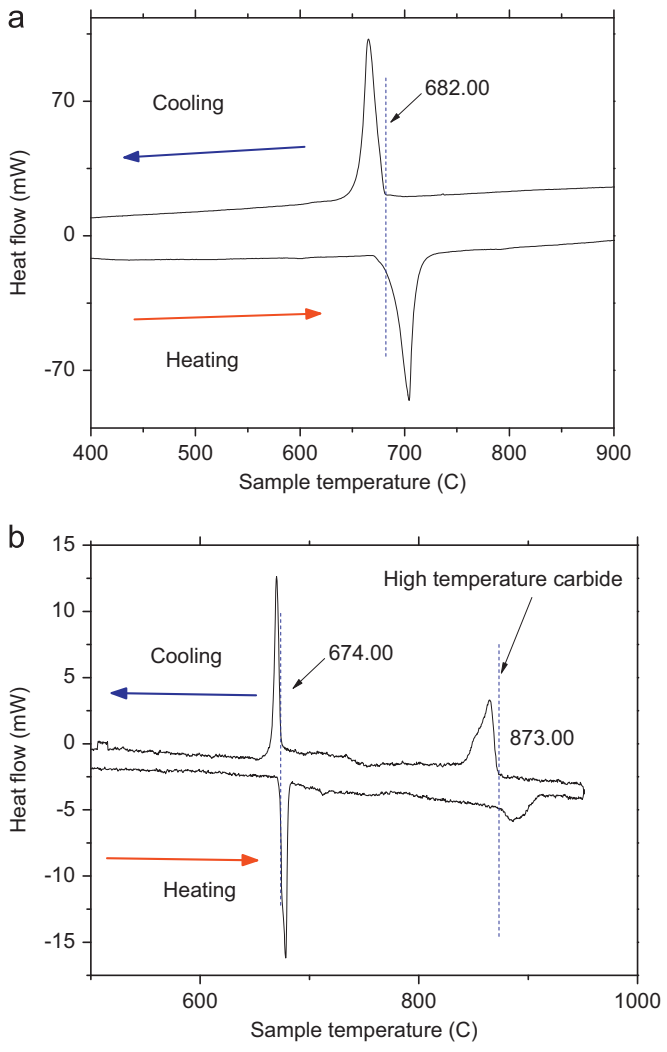

Fig. 2. DSC results of the eutectic sample composed of 27.8 at% Mn using (a) alumina crucibles, and (b) graphite crucibles.

3. Thermodynamic modeling

The Gibbs Energy functions used for the pure elements (Mn and Nd) were taken from the SGTE (Scientific Group Thermodata Europe) compilation of Dinsdale [20]. The Gibbs energy of a binary stoichiometric phase is given by:

$$G^{\phi} = x^0_{\mathrm{Mn}} G^{\phi_1}_{\mathrm{Mn}} + x^0_{\mathrm{Nd}} G^{\phi_2}_{\mathrm{Nd}} + \Delta G_f \quad (1)$$

where, ϕ denotes the phase of interest, x_{Mn} and x_{Nd} are mole fractions which are given by the stoichiometry of the compound, ${}^0G^{\phi_1}_{\mathrm{Mn}}$, and ${}^0G^{\phi_1}_{\mathrm{Nd}}$ are Gibbs energy of elements Mn and Nd in their standard state, and ΔG_f represents the Gibbs energy of formation of the stoichiometric compound. Here $\Delta G_f = a + bT$, and the parameters a and b were obtained by thermodynamic optimization using the calculated enthalpy of formation of the intermetallic compounds by first-principles calculations and the experimental phase diagram data from Saccone et al. [4] and the current work.

The Gibbs energy of the terminal solid solution phases are described by the following equation:

$$G^{\phi} = x^0_{\mathrm{Mn}} G^{\phi}_{\mathrm{Mn}} + x^0_{\mathrm{Mn}} G^{\phi}_{\mathrm{Nd}} + RT[x_{\mathrm{Mn}} \ln x_{\mathrm{Mn}} + x_{\mathrm{Nd}} \ln x_{\mathrm{Nd}}] + {}^{\mathrm{ex}}G^{\phi} \quad (2)$$

The first two terms on the right hand side of Eq. (2) represent the Gibbs energy of the mechanical mixture of the components, the third term is the ideal Gibbs energy of mixing, and the fourth term is the excess Gibbs energy. For terminal solid solutions, Bragg–Williams model was used in the form of Redlich–Kister polynomial as:

$${}^{\mathrm{ex}}G^{\phi} = x_{\mathrm{Mn}} \times x_{\mathrm{Nd}} \sum_{n=0}^{n=m} {}^{n}L^{\phi}_{\mathrm{Mn,Nd}} (x_{\mathrm{Mn}} - x_{\mathrm{Nd}})^n \quad (3)$$

$${}^{n}L^{\phi}_{\mathrm{Mn,Nd}} = a_n + b_n T \quad (4)$$

where a_n and b_n are respectively the enthalpy and entropy contributed to the excess Gibbs energy. These parameters were optimized considering the experimental phase diagram and thermodynamic data.

The modified quasi-chemical model [21–23] was chosen to describe the liquid phase because it is more physically sound in describing the liquid phase than the conventional Bragg–Williams model [18]. The modified quasi-chemical model has three distinct characteristics: (i) It permits the composition of maximum short range ordering in a binary system to be freely chosen. (ii) It expresses the energy of pair formation as a function of composition which can be expanded as a polynomial in the pair fraction. Also, the coordination numbers are permitted to vary with the composition. (iii) The model can be extended to multicomponent

Table 2
The experimental results obtained by ICP, DSC and EPMA.

Sample	Actual composition (at%)		Phase transformation temperatures (°C)	Annealing		Phase composition (at%)		
	Mn	Nd		*T* (°C)	Days	Phases	Mn	Nd
2.5 at% Mn	2.94	97.06	633					
			796					
			837					
			968					
5 at% Mn	4.6	95.4	644	400	74	DHCP-Nd	1.63	98.37
			783			$Mn_{17}Nd_2$	88.5	11.5
			868					
			932					
10 at% Mn	10.46	89.54	679	600	30	DHCP-Nd	1.2	98.8
			726			Mn_2Nd	65	35
			857			$Mn_{23}Nd_6$	77.5	32.5
15 at% Mn	15.41	84.59	682	600	30	DHCP-Nd	1.19	98.81
			725			Mn_2Nd	65.5	34.5
			790			$Mn_{23}Nd_6$	78.0	22.0
20 at% Mn	21.96	78.04	685					
			746					
27 at% Mn	27.8	72.2	682					
35 at% Mn	36.66	63.34	685					
			764					
45 at% Mn	45.59	54.41	682					
			823					
55 at% Mn	53.27	46.73	685					
			850					
			889					
65 at% Mn	64.23	35.77	685			Nd	1.0	99.0
			851	650	30	DHCP-Nd	2.16	97.84
			936			Mn_2Nd	66.5	33.5
				550	21	DHCP-Nd	1.86	98.14
						$Mn_{23}Nd_6$	78.9	21.1
75 at% Mn	75.58	24.42	819	750	31	Mn_2Nd	66.5	33.5
			849			$Mn_{23}Nd_6$	79.3	20.7
			944	600	30	Mn_2Nd	66.3	33.7
			999			$Mn_{23}Nd_6$	79.3	20.7
						$Mn_{17}Nd_2$	87.3	12.7
87 at% Mn	86.54	13.46	726	750	31	$Mn_{23}Nd_6$	79.3	20.7
			945			$Mn_{17}Nd_2$	89.3	10.7
			1025	600	30	$Mn_{23}Nd_6$	79.5	20.5
			1072			$Mn_{17}Nd_2$	89.5	10.5
						Mn	100	0
				400	68	DHCP-Nd	-	-
						$Mn_{23}Nd_6$	78	22
						$Mn_{17}Nd_2$	88.5	11.5
						Mn	100	0
88.5 at% Mn	88.1	11.9	730	600	68	$Mn_{23}Nd_6$	79.5	20.5
			944			$Mn_{17}Nd_2$	89.5	10.5
			1026			Mn	100	0
			1090					
				400	68	DHCP-Nd	-	-
						$Mn_{23}Nd_6$	79.5	20.5
						$Mn_{17}Nd_2$	89.5	10.5
						Mn	100	0
92 at% Mn	92.41	7.59	724	750	31	$Mn_{17}Nd_2$	89.5	10.5
			956			Mn	100	0
			1066					
			1119	600	30	$Mn_{23}Nd_6$	79.5	20.5
			1136			$Mn_{17}Nd_2$	89.5	10.5
						Mn	100	0
				400	74	$Mn_{23}Nd_6$	79	21
						$Mn_{17}Nd_2$	89	11
						Mn	100	0
96 at% Mn	95.42	4.58	728					
			1022					
			1055					
			1193					

systems. For instance, the Mn–Nd system is a constituent binary of the Mg–Mn–Nd ternary system; the liquid phase of the other binaries (Mg–Nd and Mg–Mn) was described using the modified quasi-chemical model. Therefore, it is preferable to model the Mn–Nd liquid using the modified quasi-chemical model for extrapolation compatibility. The model has been discussed extensively in the literature [21–23] and will be outlined briefly here. According to [21], the Gibbs energy for a solution is given by:

$$g = (nMng^0_{Mn} + n_{Nd}g^0_{Nd}) - T\Delta S^{config} + (n^{MnNd}/2)\Delta g_{MnNd} \quad (5)$$

where g^0_{Mn} and g^0_{Nd} are the molar Gibbs energies of the pure metals, ΔS^{config} is the configurational entropy of mixing given by

randomly distributing the (*Mn–Mn*), (*Nd–Nd*) and (*Mn–Nd*) pairs. The energy of pair formation can be expressed by the following equation:

$$\Delta g_{\mathrm{MnNd}} = \Delta g^{0}_{\mathrm{MnNd}} + \sum_{Mn\geq 1} g^{\mathrm{Mn0}}_{\mathrm{MnNd}} X^{\mathrm{Mn}}_{\mathrm{MnMn}} + \sum_{Nd\geq 1} g^{\mathrm{0Nd}}_{\mathrm{MnNd}} X^{\mathrm{Nd}}_{\mathrm{NdNd}} \quad (6)$$

where, $\Delta g^{0}_{\mathrm{MnNd}}$, Δg^{Mn0}_{MnNd} and $\Delta g^{0\mathrm{Nd}}_{\mathrm{MnNd}}$ are the parameters of the model and can be expressed as functions of temperature $\Delta g^{0}_{\mathrm{MnNd}} = a + bT$. Where a and b are the enthalpy and entropy contributed to the Gibbs energy, respectively. Also, the atom to atom coordination numbers Z_{Mn} and Z_{Nd}, can be expressed as function of composition as:

$$\frac{1}{Z_{\mathrm{Mn}}} = \frac{1}{Z^{\mathrm{Mn}}_{\mathrm{MnMn}}}\left(\frac{2n_{\mathrm{MnMn}}}{2n_{\mathrm{MnMn}} + n_{\mathrm{NdMn}}}\right) + \frac{1}{Z^{\mathrm{Mn}}_{\mathrm{MnNd}}}\left(\frac{n_{\mathrm{MnNd}}}{2n_{\mathrm{MnMn}} + n_{\mathrm{MnNd}}}\right) \quad (7)$$

$$\frac{1}{Z_{Nd}} = \frac{1}{Z^{\mathrm{Nd}}_{\mathrm{NdNd}}}\left(\frac{2n_{\mathrm{NdNd}}}{2n_{\mathrm{NdNd}} + n_{\mathrm{MnNd}}}\right) + \frac{1}{Z^{\mathrm{Nd}}_{\mathrm{MnNd}}}\left(\frac{n_{\mathrm{MnNd}}}{2n_{\mathrm{NdNd}} + n_{\mathrm{MnNd}}}\right) \quad (8)$$

where n_{MnNd} is the number of moles of (*Mn–Nd*) pairs, $Z^{\mathrm{Mn}}_{\mathrm{MnMn}}$ and $Z^{\mathrm{Mn}}_{\mathrm{MnNd}}$ are the coordination numbers when all nearest neighbours of an Mn atom are Mn or Nd atoms, respectively. The values of $Z^{\mathrm{Mn}}_{\mathrm{MnNd}}$ and $Z^{\mathrm{Nd}}_{\mathrm{NdMn}}$ are unique to the Mn–Nd binary system and should be carefully determined to fit the thermodynamic experimental data. In this work, 3 and 6 have been used for $Z^{\mathrm{Mn}}_{\mathrm{MnNd}}$ and $Z^{\mathrm{Nd}}_{\mathrm{NdMn}}$, respectively because these gave the best possible fit for the current system. Kim and Jung [18] also used same coordination numbers during their optimization. The coordination number of 6 has been used for both $Z^{\mathrm{Mn}}_{\mathrm{MnMn}}$ and $Z^{\mathrm{Nd}}_{\mathrm{NdNd}}$ since it has been used successfully during optimization of many binary systems [18,21–23].

4. First-principles calculations

Except for the enthalpy of mixing of the liquid phase [17], there are no reports on experimental thermochemical data on the system. The only available values for the enthalpy of formation of the compounds were obtained by thermodynamic calculations using CALPHAD method [18]. Therefore, in this work, numerical estimation was carried out to evaluate the enthalpy of formation of the compounds in Mn–Nd system.

The first-principles calculations were performed using the plane wave pseudopotential method within the framework of the density functional theory (DFT) as implemented in the ABINIT package [24]. A norm conserving Troullier–Martins pseudopotential [25] was employed with electronic configurations of Mn $3d^5 4s^2$ and Nd $4f^4 6s^2$. The generalized gradient approximation (GGA) according to the recipe of Perdew et al. [26] was used for the exchange correlation functional. In the present calculations, the plane-wave cut-off energy was set to be 440 eV. The special points sampling integration over the Brillouin zone was employed by using the Monkhorst–Pack (MP) method [27] with the following k-point mesh: $4\times4\times4$ for Mn, $3\times3\times2$ for Nd, $3\times3\times2$ for Mn_2Nd, $4\times4\times4$ for $Mn_{23}Nd_6$, and $3\times3\times2$ for $Mn_{17}Nd_2$. The Pulay scheme of density mixing was applied for the evaluation of energy [28]. The calculation of total energy and electronic structure were followed by cell optimization with the self-consistent-field (SCF) tolerance of 3×10^{-3} eV/cell. The final total obtained total energies are used to calculate the enthalpy of formation of each compound at 0 K using the following equation:

$$\Delta H(\mathrm{Mn}_n\mathrm{Nd}_m) = \frac{E(\mathrm{Mn}_n\mathrm{Nd}_m) - mE^0(\mathrm{Mn}) - nE^0(\mathrm{Nd})}{n+m} \quad (9)$$

where E is the calculated total energy of the compound and E^0 is the total energy of the elements in their standard reference state. Each structure is fully relaxed to their equilibrium geometry. All atomic positions in the lattice were relaxed according to the total energy and force using the BFGS [27] scheme based on the cell optimization criterion (RMS force of 0.01 eV/Å, stress of 0.05 GPa).

5. Results and discussion

5.1. Experimental results

The entire composition range of the Mn–Nd system was investigated experimentally by means of ICP, XRD, DSC, and SEM/EPMA techniques. 15 key samples of collected compositions and a solid–solid diffusion couple of Mn to Nd end-members were annealed and analyzed. The experimental results of phase transformations and phase identification based on DSC and EPMA studies are summarized in Table 2.

5.1.1. The Mn–Nd liquidus

The phase transformation temperatures obtained by DSC experiments were recorded based on the best match between the onset peaks of heating and cooling cycles. Fig. 3 shows results of Saccone et al. [4], and the liquidus line of Kirchmayr and Lugscheider [11] superimposed on the experimental results and the re-optimized phase diagram from the current work.

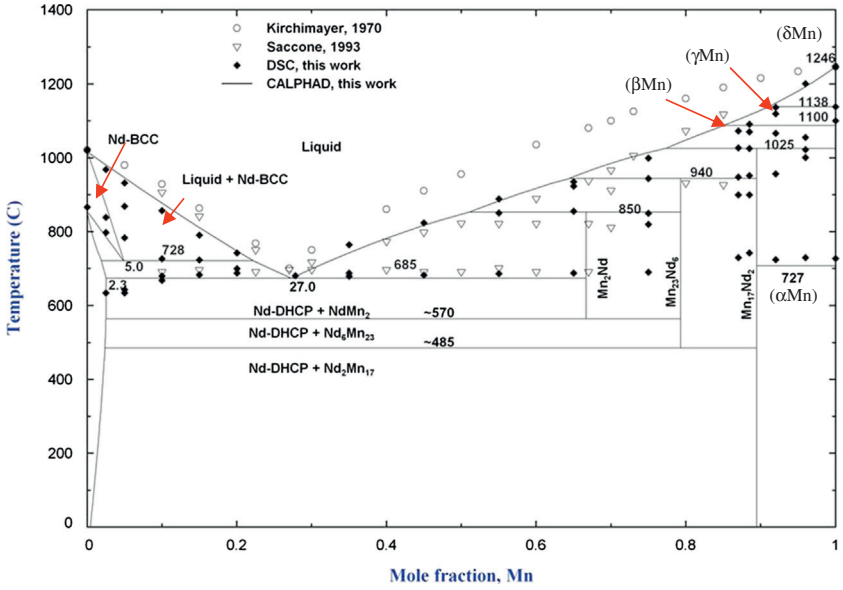

Fig. 3. The optimized Mn–Nd phase diagram along with DSC results of the current work, the partial Mn–Nd phase diagram of [4] and the liquidus line of [11].

The pure Nd was found to melt at 1021 °C and undergoes a DHCP→BCC phase transformation at 862 °C. These temperatures agree with the ones reported in Massalski [29]. On the other hand, pure Mn melts at 1246 °C and undergoes three polymorphic transformations, α→β at 727 °C, β→γ at 1100 °C, and γ→δ at 1138 °C. Based on the similarity with the Mn–Pr [3] and Ce–Mn [30] systems and on the current results, Nd-rich alloys exhibit a peritectic reaction L+DHCP-Nd⇔BCC-Nd at 728 °C. The solubility of Mn in BCC-Nd at this temperature was estimated to be 5.0 at% Mn. In addition, the terminal solid solubility of Mn in DHCP-Nd was determined at the 685 °C eutectic temperature to be 2.3 at% Mn. The allotropic transformation temperatures in the Mn-rich side were unaffected by the addition of Nd. This was confirmed by thermal analysis of two Mn-rich alloys; 92 and 96 at% Mn using DSC. The thermal arrests associated with the Mn allotropic transformations, obtained in this work, agree very well with the values reported by Palenzona and Cirafici [31]. The negligible solubility of Nd in Mn was confirmed by EPMA studies of the Mn-rich samples in both as-cast and annealed conditions.

To conform with Okamoto's [14] suggestion, the limiting slope of the liquidus boundaries [32,33] closer to the Nd terminal side, was modified based on the current DSC results. This modification supports the presence of BCC-Nd solid solution. The DSC experiments of all sample compositions showed a lower liquidus line than that reported in the work of [11,13] and agree with the DTA results of Saccone et al. [4].

From Table 2, the DSC measurements associated with the extension of γ-Mn transformation line in the Mn-rich alloys containing 88.5, 92, and 96 at% Mn were recorded at less than 1100 °C. That might be attributed to the supercooling effect. Because these alloys have high melting temperature, the amount of overheating of the melt affects the nucleation and growth of crystals of different phases upon cooling [34]. As a result, a significant shift in the DSC peaks can be observed.

5.1.2. The DHCP-Nd–Mn_2Nd eutectic

The temperature of the DHCP-Nd–Mn_2Nd eutectic (27 at% Mn) was determined to be 685 °C, which is considerably lower than the reported value by Saccone et al. [4] of 695 °C. The latter value, however, varied slightly, from 700 °C [11,13] to 695 °C.

A sample with actual composition of 27.8 at% Mn furnace cooled from the melt gave the eutectic microstructure shown in Fig. 4. Both fine and coarse eutectic dendrites were observed. The fine eutectic dendrites are in the form of two alternating layers of DHCP-Nd and Mn_2Nd. The coarse eutectic dendrites formed due to the shift in sample composition by 0.8 at% from the actual eutectic composition of 27.0 at% Mn that is confirmed in the literature [4,11,13]. Because of the shift in composition, Mn_2Nd precipitated first to form coarse dendrites (the black phase in Fig. 4).

5.1.3. The intermetallic compounds

Three intermetallic compounds (Mn_2Nd, $Mn_{23}Nd_6$, and $Mn_{17}Nd_2$) peritectically formed at 850, 940, and 1025 °C, respectively. In agreement with Makhalenko and Kuz'ma [13] and Saccone et al. [4], the compound $Mn_{12}Nd$ was not observed. The peritectic temperatures were determined from the thermal arrests associated with the phase transformations during heating and cooling cycles using different scanning speeds of 5, 10, and 15 °C/min. Small temperature variations in the range of ± 3 °C were observed due to changing the heating and cooling rates. Systematic metallographic studies were performed to verify the phase equilibria of the intermetallic phases. Three samples of 75.58, 86.5 and 92.41 at% Mn were brought to equilibrium by annealing at 750 °C for 31 days. Fig. 5(a–c) shows the two-phase equilibria in the annealed samples. Mn_2Nd and $Mn_{23}Nd_6$ were found in equilibrium in the first sample, $Mn_{23}Nd_6$ and $Mn_{17}Nd_2$ in the second sample, and $Mn_{17}Nd_2$ and α-Mn in the third sample.

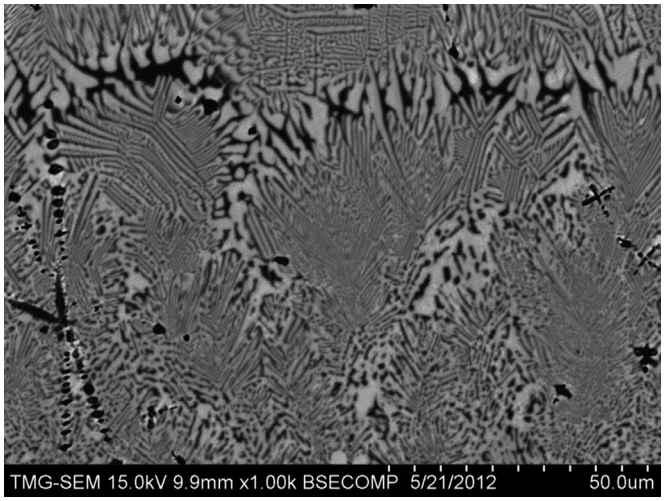

Fig. 4. SEM micrograph for the DHCP-Nd-Mn_2Nd eutectic sample at 27.8 at% Mn.

5.1.4. $Mn_{17}Nd_2$ compound

$Mn_{17}Nd_2$ was not reported in the previous versions of the Mn–Nd phase diagram [4,11,13] and $Mn_{12}Nd$ was reported instead [11,13,16]. In the present work, the presence of $Mn_{17}Nd_2$ was confirmed by EPMA measurements of annealed key alloys and diffusion couple. The crystal structure was determined by X-ray diffraction. Tsvyashchenko and Popova [9] discovered a $Mn_{17}Yb_2$ phase with

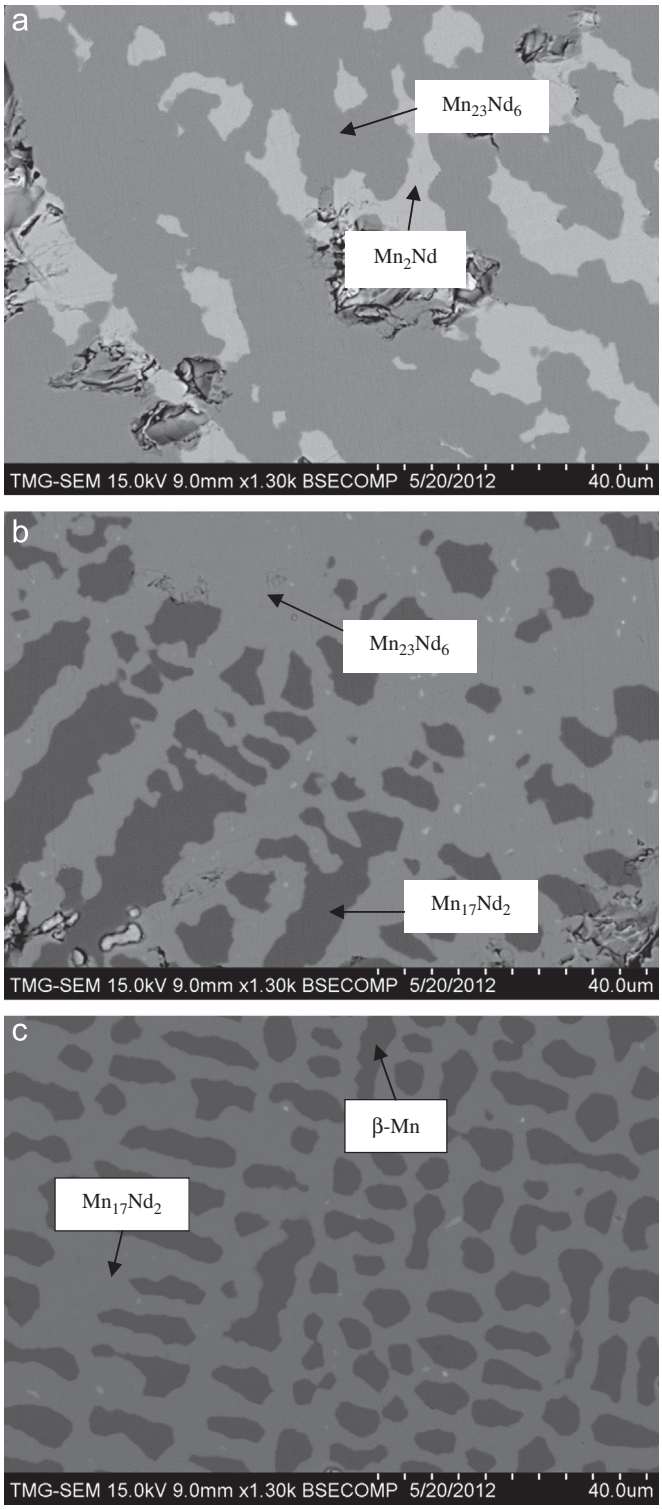

Fig. 5. Equilibrated phases in (a) 75.58 at% Mn, (b) 86.5 at% Mn and (c) 92.41 at% Mn samples annealed at 750 °C for 31 days.

Th_2Ni_{17} type structure (Table 1). They proposed that the phase was formed at high pressure of 7.7 GPa and a temperature of 1200 °C. Fig. 6 shows the peritectic formation of $Mn_{17}Nd_2$, according to the equilibrium reaction $Mn_{17}Nd_2 \Leftrightarrow L+\beta$-Mn at 1025 °C, from a sample containing 88.5 at% Mn annealed at 850 °C for 31 days.

Moreover, the compound was observed as a thin layer in the Mn–Nd diffusion couple annealed at 650 °C for 30 days. The composition profile was measured across the diffusion layers using EPMA. Fig. 7 shows the formation of $Mn_{17}Nd_2$ as a thin layer between the $Mn_{23}Nd_6$ layer and Mn end-member. The composition profile revealed that the phase exists with the composition of 89.5 at% Mn, which corresponds to the Mn:Nd 17:2 stoichiometry. No evidence of solubility of Nd in Mn up to 850 °C was detected.

Further confirmation of the existence of $Mn_{17}Nd_2$ was obtained from the XRD results of a sample containing 92 at% Mn annealed at 400 °C for 74 days. The XRD spectrum of Fig. 8 shows peaks of a small amount of $Mn_{23}Nd_6$, pure Mn, and $Mn_{17}Nd_2$. This was also confirmed using EPMA studies on the annealed sample shown in Fig. 9.

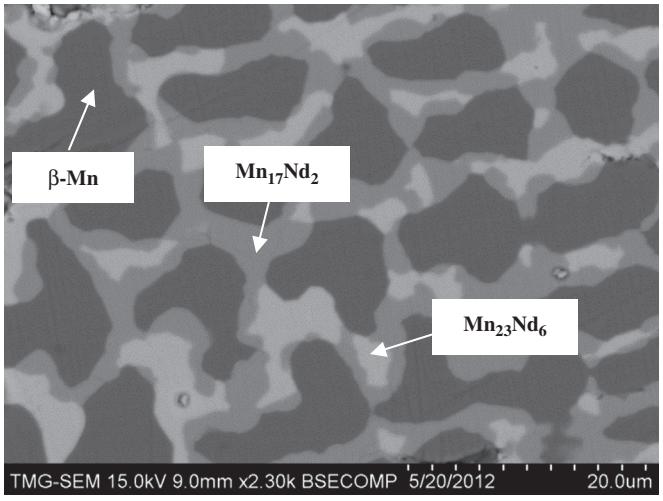

Fig. 6. The peritectic formation of $Mn_{17}Nd_2$.

Three phases were seen in the binary alloy shown in Fig. 9 because the alloys in this system need very long annealing time to reach equilibrium due to the presence of many peritectic reactions. For example in this micrograph, it can be seen that 74 days were not enough for the complete peritectic formation of the $Mn_{17}Nd_2$ compound.

X-ray diffraction analysis revealed the structure type of $Mn_{17}Nd_2$ as $Zn_{17}Th_2$ with $a=8.79085$ Å and $c=12.6979$ Å. The lattice parameters were computed through a least-square interpolation using X′pert Highscore plus software [19]. In all XRD experiments, Rietveld quantitative analysis was performed to measure the relative amounts of the phases existing in each sample as shown in Fig. 10.

5.1.5. *Mn_2Nd and $Mn_{23}Nd_6$ eutectoidal decomposition*

In agreement with Saccone et al. [4], Mn_2Nd and $Mn_{23}Nd_6$ were found to decompose eutectoidally at ~580 and ~480 °C, respectively. Because of the difficulty of detecting the solid–solid phase transformation temperatures [35], the eutectoidal decomposition temperatures could not be determined by DSC experiments, even at very slow scanning speeds. Therefore, the eutectoidal decompositions of Mn_2Nd and $Mn_{23}Nd_6$ were determined using systematic annealing and quenching procedures. The decomposition range of Mn_2Nd was determined to be in the temperature range of 600–650 °C. The 65 at% Mn sample was annealed at 650 °C for 30 days in the same quartz tube capsule as a diffusion couple designed to be annealed for 30 days. The EPMA results showed that Mn_2Nd was in equilibrium with an DHCP-Nd solid solution containing 2.16 at% Mn. Another sample with the same composition was annealed at 550 °C for 21 days since the annealing time was found sufficient to reach equilibrium. In case that the equilibrium was not reached, the samples must be returned to the furnace for longer annealing time. The microstructure shows that $Mn_{23}Nd_6$, instead of Mn_2Nd, is in equilibrium with DHCP-Nd, containing 1.86 at% Mn, as shown in Fig. 11(a) and (b).

For the above-mentioned sample, the equilibrium was reached at 550 °C after 21 days of annealing due to the fast reformation of $Mn_{23}Nd_6$ phase, since the cast structure contained larger amount of $Mn_{23}Nd_6$. However, at 650 °C, 30 days of annealing were necessary to form Mn_2Nd compound through a solid-state reaction which requires longer time to achieve.

The eutectoidal decomposition range of $Mn_{23}Nd_6$ was confirmed to be in the temperature range of 400–550 °C, by bringing the Nd-rich sample of 5 at% Mn to equilibrium by annealing at 400 °C for 74 days. Very fine phase features were observed because of the dominant DHCP-Nd solid solution. Among these fine features, $Mn_{17}Nd_2$ formed a needle-like morphology within an DHCP-Nd solid solution matrix containing 1.63 at% Mn, as shown in Fig. 12. No traces of $Mn_{23}Nd_6$ could be found in this sample after annealing.

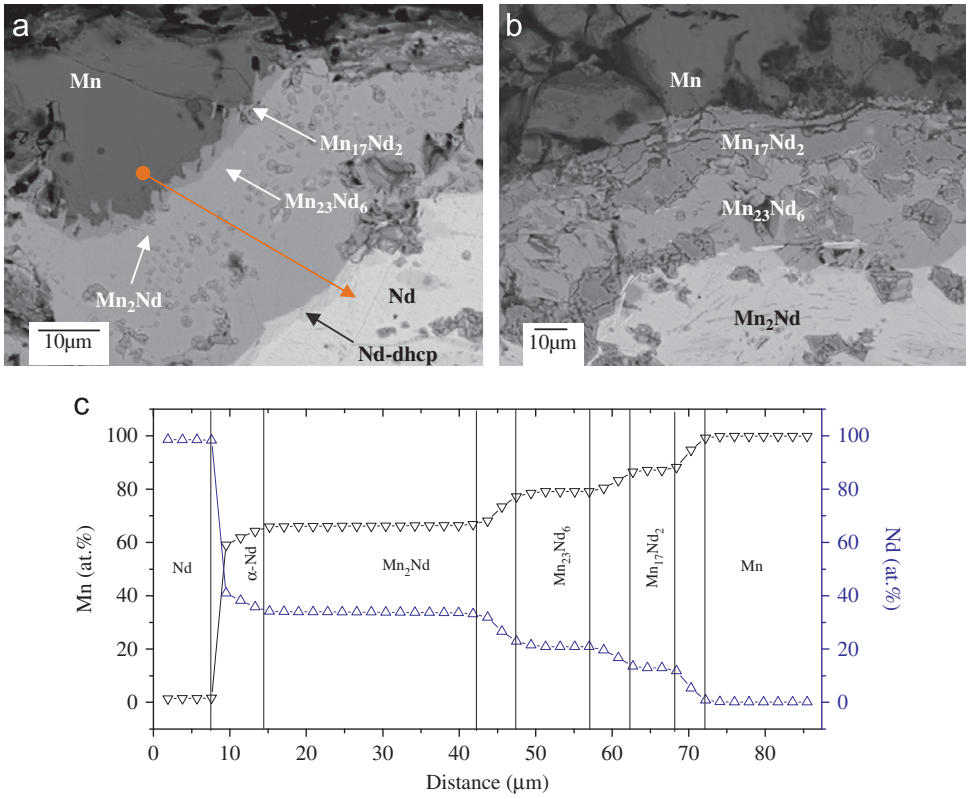

Fig. 7. (a) and (b) SEM micrograph of Mn–Nd diffusion couple annealed at 650 °C for 30 days showing the three intermetallics, and (c) the composition profile of the same diffusion couple.

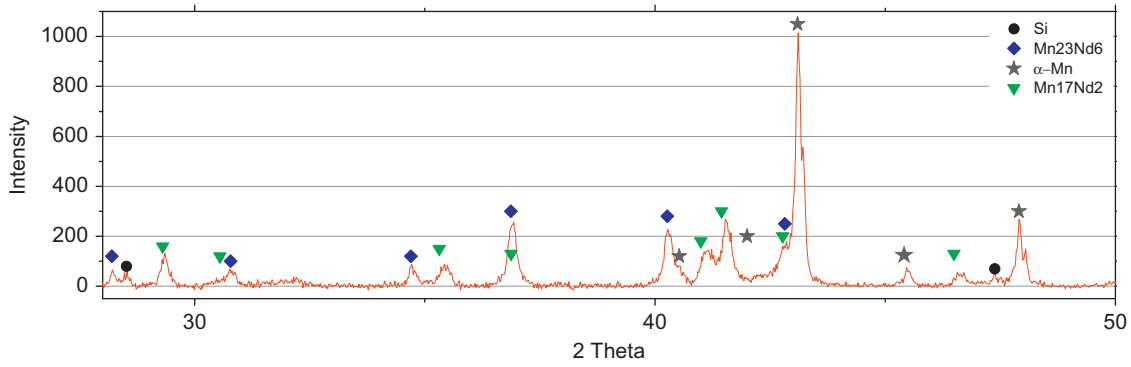

Fig. 8. XRD spectrum of 92 at% Mn sample powder annealed at 400 °C for 27 days.

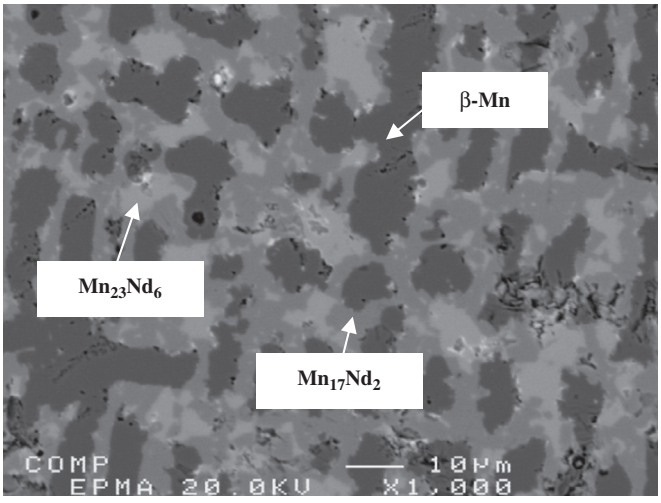

Fig. 9. Sample of 92 at% Mn annealed at 400 °C for 74 days. The peritectic structure of Mn dendrites surrounded by $Mn_{17}Nd_2$, and the brighter phase is the $Mn_{23}Nd_6$.

It was pointed out by [3,4,13] that the phase transformation rates in this type of alloys are very slow; hence, annealing for long times was required to have equilibrated samples. Despite the long annealing time, the binary alloys were found to attain more than two phases at lower temperatures. Hence, the phase morphologies and phase equilibria were understood through annealing the same sample at different temperatures. Three phases were observed in the two hypoeutectic samples; namely, 10 and 15 at%, after annealing at 600 °C for 30 days. According to the phase equilibria and the samples compositions, it is impossible to have the compound $Mn_{23}Nd_6$ during solidification. The phase existence was proposed due to the eutectoidal decomposition of the Mn_2Nd at 600 °C. Because of the slow solid–solid transformation kinetics, three phases were observed due to the incomplete decomposition of Mn_2nd to $Mn_{23}Nd_6$. However, this can provide more confidence on the Mn_2Nd eutectoidal decomposition.

Some authors [4,13] reported the formation of a $ThMn_{12}$-type structure for a ternary compound when using Al_2O_3 crucibles for thermal analysis experiments. In the present work, the DSC experiments were carried out on the full range of system compositions using Al_2O_3 crucibles. No traces of a $Mn_{12}Nd$ phase were observed by either XRD or EPMA studies. The maximum solubility of 2.3 at% Mn in DHCP-Nd, observed by the EPMA study on the eutectic sample containing 27.8 at% Mn, in the as-cast condition. In contrast, the maximum solubility of Mn in BCC-Nd was determined as 5.0 at% Mn by extrapolating from the DSC results.

5.2. Thermodynamic modeling

The Mn–Nd system has been thermodynamically modeled using the CALPHAD approach. FactSage software 6.3 was used for the thermodynamic optimization. The experimental data for the enthalpy of mixing of the liquid was obtained from Ivanov et al. [17]. The enthalpy of formation of the intermetallic compounds was estimated using first-principles calculations. These values were used as preliminary approximation during optimization. Also, the experimental phase diagram data were provided from the current work and from Saccone et al. [4]. The calculated phase diagram in Fig. 3 shows reasonable agreement with the experimental data. However, it deviates from those of Kirchmayr and Lugscheider [11] who reported higher liquidus for the entire composition range. The optimized parameters for the liquid, terminal solid solutions and intermetallic compounds are given in Table 3. The invariant equilibria in the Mn–Nd system are given in Table 4. The maximum solubility of Mn in DHCP-Nd has been calculated as 2.3 at% at the eutectic temperature. The solubility of Nd in Mn is negligible and is not recorded here. The eutectic reaction occurs at 685 °C and 27 at% Mn.

The DSC curves were analysed carefully. No clear peaks indicating the solid–solid transformation were detected. Therefore, no experimental points associated with the eutectoidal decomposition of the two compounds Mn_2Nd and $Mn_{23}Nd_6$ were shown in the optimised phase diagram in Fig. 3. However, the decomposition temperature ranges were obtained through a series of annealing and quenching experiments.

Ivanov et al. [17] measured the partial enthalpy of mixing of Nd in the range of 0 to 25 at% of Nd and that of Mn from 42 at% to the pure Nd. Their [17] reported values were used during the optimization process. As it can be seen in Fig. 13(a), the present calculation can reproduce the partial enthalpies of Nd and Mn within the experimental error. Based on their experimental data, Ivanov et al. [17] also, calculated the integral enthalpy of mixing of the entire Mn–Nd liquid assuming that the change of partial enthalpy is negligible in the temperature range between 1550 and 1600 K. The enthalpy of mixing curve produced in this work shows reasonable agreement with these results [17] as shown in Fig. 13(b).

First-principles calculations were used to determine the enthalpy of formation of the intermetallic compounds. The calculated values were used as first approximation during optimization of the system. The values were adjusted to achieve consistency between the calculated and experimentally obtained phase diagrams. First-principles calculations were found in reasonable agreement with the current CALPHAD results except for $Mn_{17}Nd_2$. The calculated values of enthalpy of formation using first-principles calculations, and CALPHAD are summarized in Table 5.

Fig. 14 shows a comparison between the enthalpy of formation of the intermetallic compounds obtained using CALPHAD approach and first-principles calculations in this work compared to those reported in the work of Kim and Jung [18].

5.3. First-principles calculations

First-principles calculations were used to determine the enthalpy of formation of the intermetallic compounds. The calculated values were used as first approximation during optimization of the system. The values were adjusted to achieve consistency between the calculated and experimentally obtained phase diagrams. First-principles calculations were found in reasonable agreement with the current CALPHAD results except for Mn17Nd2. The calculated values of enthalpy of formation using first-principles calculations, and CALPHAD are summarized in Table 5.

6. Summary

A self-consistent Mn–Nd phase diagram was obtained based on experimental investigation and thermodynamic modeling. A diffusion couple from pure Mn to pure Nd was annealed at 650 °C and 15 key samples were investigated using ICP, DSC, XRD, and SEM/EPMA. The peritectic formation of the intermetallic compounds was confirmed. The liquidus line was reassessed using DSC. The limiting slopes of the new liquidus support the existence of BCC-Nd solid solution. The composition profiles obtained from the diffusion couple revealed the presence of the three intermetallic compounds, as well as the terminal solid solubility of Mn in DHCP-Nd. A systematic

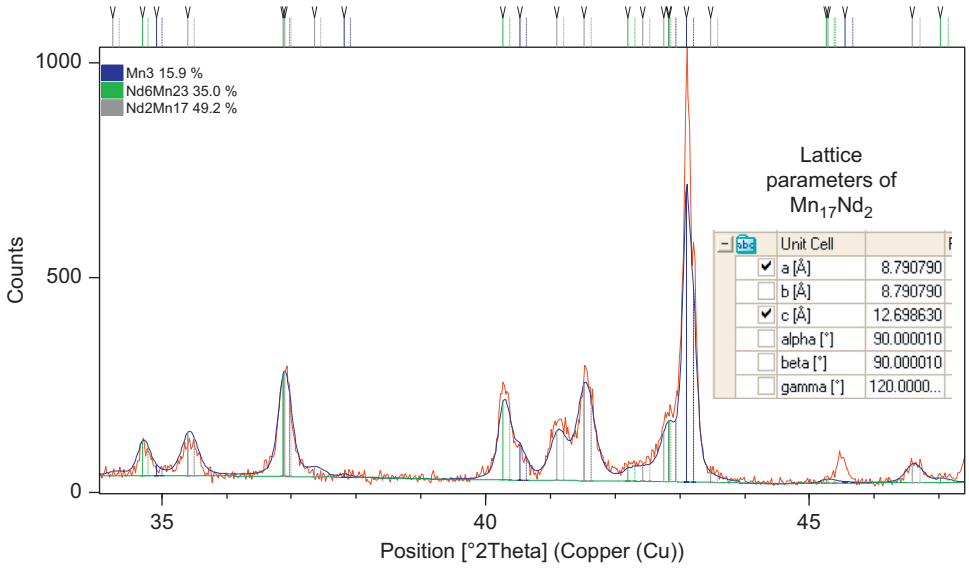

Fig. 10. The observed diffraction intensities compared with the calculated values for a sample containing 92 at% Mn annealed at 400 °C for 27 days. The calculated lattice parameters of $Mn_{17}Nd_2$ are shown in the right side.

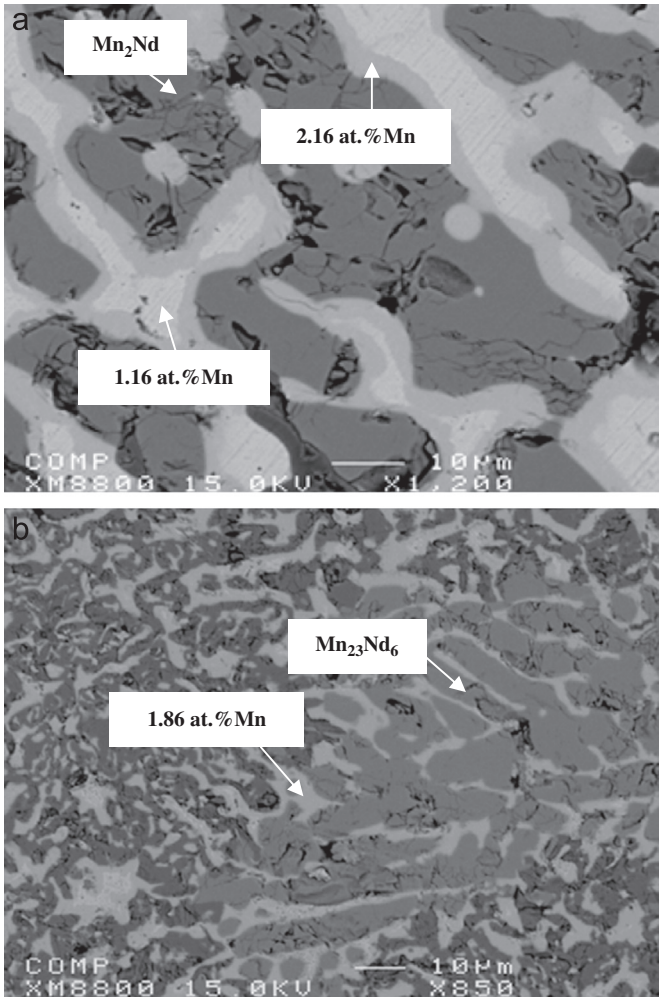

Fig. 11. SEM micrograph of 65 at% Mn (a) annealed at 650 °C for 30 days showing Mn_2Nd and DHCP-Nd with 2.16 at% Mn, and (b) annealed at 550 °C for 21 days showing $Mn_{23}Nd_6$ and DHCP-Nd with 1.86 at% Mn.

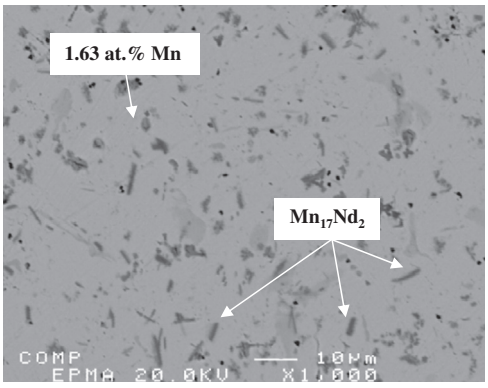

Fig. 12. SEM micrograph of 5 at% Mn annealed at 400 °C for 74 days showing the columnar $Mn_{17}Nd_2$ and DHCP-Nd with 1.63 at% Mn.

Table 3
Optimized model parameters for the Mn–Nd system.

Phase	Terms	a (J/mol/atom)	b (J/mol/atom/K)
		$Z^{Mn}_{MnNd}=3$; $Z^{Nn}_{MnNd}=6$	
Liquid	Δg^{0}_{MnNd}	3849.28	−3.10
	Δg^{Mn0}_{MnNd}	−5860.12	6.28
	Δg^{0Nd}_{MnNd}	836.80	−0.33
Nd-dhcp	${}^{0}L^{Nd\text{-}dhcp}$	1255.20	41.44
	${}^{1}L^{Nd\text{-}dhcp}$	0	−16.74
Nd-bcc	${}^{0}L^{Nd\text{-}bcc}$	36416.46	10.46
	${}^{1}L^{Nd\text{-}bcc}$	33067.82	0.00
Mn_2Nd	Δg_f	4200.00	−5.27
$Mn_{23}Nd_6$	Δg_f	2001.85	−2.65
$Mn_{17}Nd_2$	Δg_f	86.84	−0.102

procedure of microstructural studies (by annealing the same sample at different temperatures) was adopted to confirm the eutectoidal decomposition of two intermetallic compounds, Mn_2Nd and $Mn_{23}Nd_6$ at 600–650 and 400–550 °C, respectively. A new peritectically formed

Table 4
Comparison between the experimental and calculated invariant points in the Mn–Nd phase diagram.

Reaction	Reaction type	Experimental points				Calculated points			
		T (°C)	x (Mn)			T (°C)	x (Mn)		
L⇔Mn_2Nd+DHCP-Nd	Eutectic	685	0.278	0.660	0.023	682	0.268	0.660	0.022
L+$Mn_{23}Nd_6$⇔ Mn_2Nd	Peritectic	850	0.525	0.791	0.660	849	0.523	0.791	0.660
L+$Mn_{17}Nd_2$⇔ $Mn_{23}Nd_6$	Peritectic	940	0.676	0.895	0.791	958	0.670	0.895	0.791
L+βMn⇔ $Mn_{17}Nd_2$	Peritectic	1025	0.781	1.00	0.895	1025	0.780	1.00	0.895
BCC-Nd⇔ DHCP-Nd+L	Peritectic	728	0.050	0.023	0.221	728	0.045	0.022	0.220
Mn_2Nd⇔ $Mn_{23}Nd_6$+ DHCP-Nd	Eutectoid	~600	0.660	0.791	0.023	561	0.660	0.791	0.022
$Mn_{23}Nd_6$⇔ $Mn_{17}Nd_2$+ DHCP-Nd	Eutectoid	~500	0.791	0.895	0.023	485	0.791	0.895	0.022

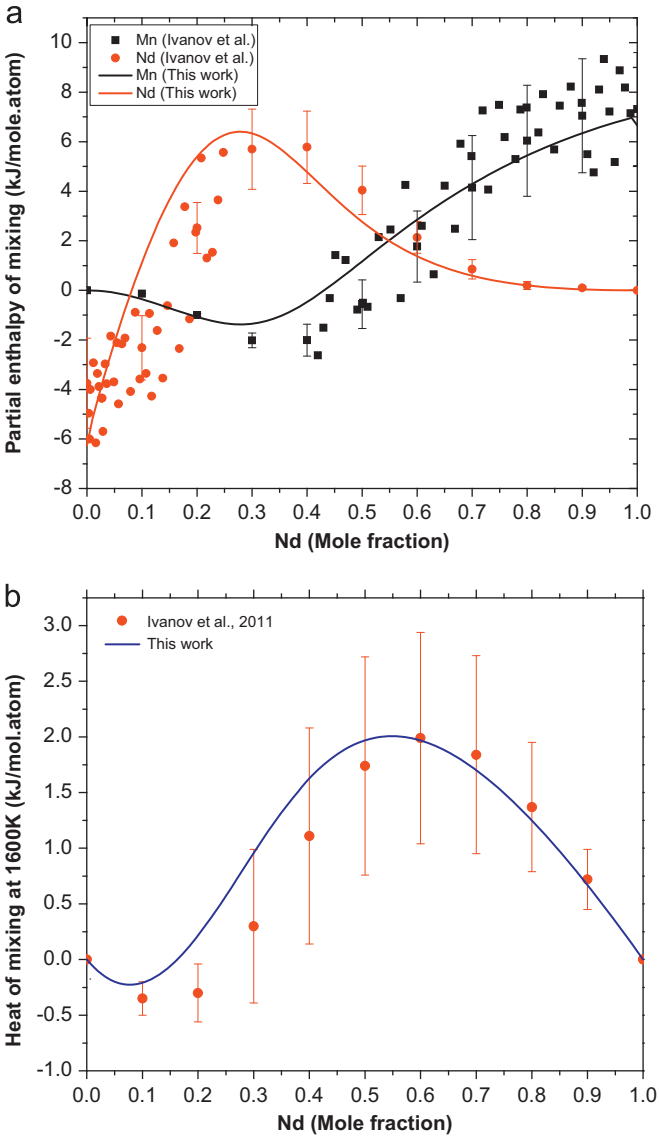

Fig. 13. Calculated (a) partial enthalpies of mixing of liquid Mn–Nd, and (b) integral enthalpy of mixing of liquid Mn–Nd at 1600 K compared with [7].

compound with $Zn_{17}Th_2$-type structure was observed in the Mn-rich side. The phase was assigned $Mn_{17}Nd_2$ formula based on EPMA and XRD studies. First-principles calculations and CALPHAD method were performed to evaluate the enthalpy of formation of the compounds. The modified quasi-chemical model was used to describe the liquid phase, the terminal solid solution phases in the Nd side were described as substitutional solutions using the random mixing model,

Table 5
The calculated values of enthalpy of formation using different approaches.

Phase	Space group	Enthalpy of formation kJ/mol atom	
		First principles	CALPHAD
Mn_2Nd	$P6_3/mmc$	3.65	4.2
$Mn_{23}Nd_6$	Fm-3m	2.15	2.002
$Mn_{17}Nd_2$	$P6_3/mmc$	1.25	0.087

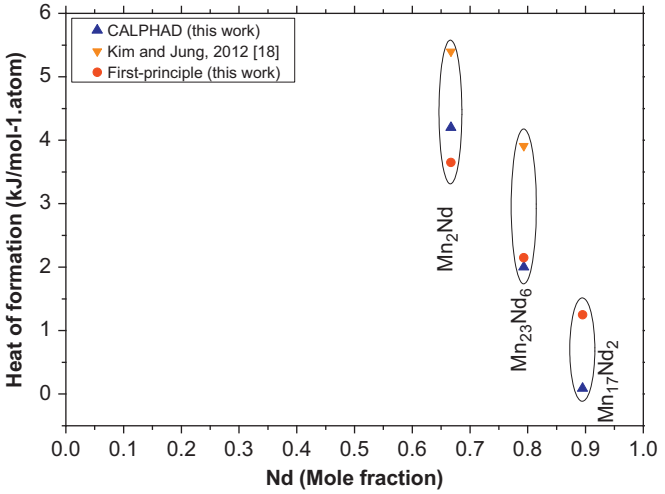

Fig. 14. Calculated enthalpy of formation of Mn–RE compounds using CALPHAD approach and first-principles calculations compared with the literature data [18].

and the three intermetallic phases were treated as stoichiometric compounds. A self-consistent set of parameters was obtained using CALPHAD approach, which can produce the phase diagram and thermodynamic properties within experimental error and in generally good agreement with the first-principles calculations.

Acknowledgement

The authors acknowledge NSERC for financial support of the project through MagNET network for excellence. Computational resources for this work were provided by the Réseau québécois de calcul de haute performance (RQCHP).

Appendix A. Supplementry material

Supplementary data associated with this article can be found in the online version at http://dx.doi.org/10.1016/j.calphad.2013.07.004.

References

[1] Wellbeloved D., Craven P., Waudby J. Manganese and manganese alloys, in: Ullmann′s Encyclopedia of Industrial Chemistry: Wiley-VCH Verlag GmbH & Co.; 2000.
[2] Matricardi L., Downing J. Manganese and manganese alloys, in: Kirk-Othmer Encyclopedia of Chemical Technology: John Wiley & Sons, Inc.; 2000, pp. 1-27.
[3] A. Saccone, S. Delfino, R. Ferro, Alloying behaviour of manganese with basic metals: Pr–Mn system, J. Less-Common Met. 108 (1985) 89–105.
[4] A. Saccone, S. Delfino, R. Ferro, Systematics of rare earth-manganese alloys: Nd–Mn phase diagram, Z. Metallkd. 84 (1993) 563–568.
[5] Y. Tagawa, J. Sakurai, Y. Komura, H. Wada, M. Shiga, Y. Nakamura, X-ray study of crystal distortions in RMn_2 compounds (R: Y, Pr, Nd, Sm and Gd), J. Phys. Soc. Jpn. 54 (1985) 591–597.
[6] P. Kripyakevich, D. Frankevich, Y. Voroshilov, Compounds with Th_6Mn_{23}-type structures in alloys of the rare-earth metals with manganese and iron, Powder Metall. Met. Ceram. 4 (1965) 915–919.
[7] M. Teslyuk, P. Kripyakevich, P. Frankevich, New laves phases containing manganese, Sov. Phys.: Crystallogr. 9 (1965) 558–559.
[8] J. Wernick, S. Haszko, Manganese rare earth compounds with the $MgZn_2$ structure, J. Phys. Chem. Solids 18 (1961) 207–209.
[9] A. Tsvyashchenko, S. Popova, High pressure phases in the Mn–Yb system, J. Less-Common Met. 90 (1983) 211–215.
[10] J. Bohlen, S. Yi, D. Letzig, K.U. Kainer, Effect of rare earth elements on the microstructure and texture development in magnesium–manganese alloys during extrusion, Mater. Sci. Eng., A 527 (2010) 7092–7098.
[11] H. Kirchmayr, W. Lugscheider, Die Zustandsbilder Neodym-Samarium- und Terbium-Mangan, Z. Metallkd. 61 (1970) 22–23. (German).
[12] J. Gröbner, A. Pisch, R. Schmid-Fetzer, Thermodynamic optimization of the systems Mn–Gd and Mn–Y using new experimental results, J. Alloys Compd. 317–318 (2001) 433–437.
[13] S. Makhalenko, Y. Kuz′ma, X-ray diffraction investigations of the Nd–Mn system, Izv. Akad. Nauk. SSSR, Neorg. Mater. 26 (1990) 2432–2433.
[14] H. Okamoto, Mn–Nd (Manganese–Neodymium), J. Phase Equilib. 13 (1992) 331–332.
[15] H. Okamoto, Comment on Mn–Nd (Manganese–Neodymium), J. Phase Equilib. 15 (1994) 568–569.
[16] J. Liu, W. Liu, L. Wang, Isothermal section of Er–Mn–Nd ternary system at 773 K, J. Rare Earths 24 (2006) 582–586.
[17] M. Ivanov, V. Berezutski, N. Usenko, Mixing enthalpies in liquid alloys of manganese with the lanthanides, Int. J. Mater. Res. 102 (2011) 277–281.
[18] J. Kim, I.-H. Jung, Critical systematic evaluation and thermodynamic optimization of the Mn–RE system: RE=La, Ce, Pr, Nd and Sm, J. Alloys Compd. 525 (2012) 191–201.
[19] PANalytical, Ver2.2b (2.2.2). In, Almelo, The Netherlands; 01-11-2006.
[20] A. Dinsdale, SGTE data for pure elements, Calphad 15 (1991) 317–425.
[21] A. Pelton, S. Degtrov, G. Eriksson, C. Robelin, Y. Dessureault, The modified quasi-chemical model: Part I. Binary solutions, Metall. Mater. Trans. 31B (2000) 651–659.
[22] P. Chartrand, A. Pelton, The modified quasi-chemical Model: Part III. Two sublattices, Metall. Mater. Trans. A 32 (2001) 1397–1407.
[23] A. Pelton, P. Chartrand, G. Eriksson, The modified quasi-chemical model: Part IV. Two-sublattice quadruplet approximation, Metall. Mater. Trans. A 32 (2001) 1409–1416.
[24] X. Gonze, G.-M. Rignanese, M. Verstraete, J.-M. Beuken, Y. Pouillon, R. Caracas, F. Jollet, M Torrent, G. Zerah, M. Mikami, P. Ghosez, M. Veithen, J.-Y. Raty, V. Olevano, F. Bruneval, L. Reining, R. Godby, G. Onida, D.R. Hamann, D.C. Allan, A brief Introduction to the ABINIT software package, Z. Kristallogr. 220 (2005) 558–562.
[25] N. Troullier, J.L. Martins, Efficient pseudopotentials for plane-wave calculations, Phys. Rev. B: Condens. Matter 43 (1991) 1993–2006.
[26] J. Perdew, K. Burke, M. Ernzerhof, Generalized gradient approximation made simple, Phys. Rev. Lett. 3865 (1996) 78.
[27] H.J. Monkhorst, J.D. Pack, Special points for Brillouin-zone integrations, Phys. Rev. B: Condens. Matter 13 (1976) 5188–5192.
[28] B. Hammer, L. Hansen, J. Nørskov, Improved adsorption energetics within density-functional theory using revised Perdew–Burke–Ernzerhof functionals, Phys. Rev. B: Condens. Matter 59 (59) (1999) 7413–7421.
[29] T. Massalski, J. Murray, L. Bennett, H. Baker, Binary Alloy Phase Diagrams, second ed., American Society for Metals, Metals Park. Ohio, 1986.
[30] B. Thamer, The system cerium–manganese in the range of 0-–20 at% manganese, J. Less-Common Met. 7 (1964) 341–346.
[31] A Palenzona, S. Cirafici, The Ce–Mn (cerium–manganese) system, J. Phase Equilib. 17 (1996) 53–56.
[32] A. Pelton, On the slopes of phase boundaries, Metall. Mater. Trans. A 19 (1988) 1819–1825.
[33] H. Okamoto, T. Massalski, Thermodynamically improbable phase diagrams, J. Phase Equilib. 12 (1991) 148–168.
[34] H. Tong, F. Shi, Dependence of supercooling of a liquid on its overheating, J. Chem. Phys. 107 (1997) 7964–7966.
[35] Y. Zhu, J. Devletian, A. Manthiram, Application of differential thermal analysis to solid–solid transitions in phase diagram determination, J. Phase Equilib. 15 (1994) 37–41.